Optical and Quantum Electronics (2021) 53:639
https://doi.org/10.1007/s11082-021-03281-4

Optimization of photonic crystal fibers for transmission of orbital angular momentum modes

Chao Liu[1] · Haihao Fu[1] · Chunjie Hu[2] · Lei Zhou[3] · Ying Shi[4] · Jingwei Lv[1] · Lin Yang[1] · Paul K. Chu[5,6,7]

Received: 13 April 2021 / Accepted: 3 October 2021 / Published online: 21 October 2021

Abstract
Photonic crystal fibers (PCFs) which can transmit orbital angular momentum (OAM) modes are attractive to optical communication due to the large capacity and flexible structure. Herein, a method is proposed to optimize a simple fiber structure by changing the thickness of the annular area. The changes in the effective index, effective index difference, dispersion, effective mode area, nonlinear coefficient, numerical aperture, mode purity, and walk-off length in the thickness range of 2.0 μm to 2.5 μm are determined, compared, and analyzed systematically. The distance between the square air holes and central air hole is the better parameter to optimize the dispersion, effective mode area, and nonlinear coefficient, whereas the radius of the central air hole is more suitable for optimizing the NA, OAM purity and walk-off length. The optimization method and results have great value pertaining to the design and improvement of PCFs for transmission of OAM modes.

Keywords Orbital angular momentum · Photonic crystal fiber · Optical fiber communication · Fiber design

✉ Chao Liu
msm-liu@126.com

1 School of Physics and Electronic Engineering, Northeast Petroleum University, Daqing 163318, People's Republic of China

2 Department of Gynaecology and Obstetrics, The Fourth Affiliated Hospital of Harbin Medical University, Harbin 150001, People's Republic of China

3 Department of Orthopedics, The Second Affiliated Hospital of Harbin Medical University, Harbin 150081, People's Republic of China

4 Institute of Unconventional Oil & Gas, Northeast Petroleum University, Daqing 163318, People's Republic of China

5 Department of Physics, City University of Hong Kong, Tat Chee Avenue, Kowloon, Hong Kong, People's Republic of China

6 Department of Materials Science and Engineering, City University of Hong Kong, Tat Chee Avenue, Kowloon, Hong Kong, People's Republic of China

7 Department of Biomedical Engineering, City University of Hong Kong, Tat Chee Avenue, Kowloon, Hong Kong, People's Republic of China

1 Introduction

The orbital angular momentum (OAM) is a new dimension in space division multiplexing and widely used in fiber optics communication because of the theoretically infinite orthogonal basis and infinite modes (Rui-Chao and Zhang 2017; Ott et al. 2008, 2003). So far, step index fibers (SIFs) (Kibler et al. 2021), graded index fibers (GIFs) (Majumdar et al. 2014), and photonic crystal fibers (PCFs) () have been proposed to propagate OAM modes. The performance of PCFs can be improved or controlled by optimizing the shape, size, number, and location of claddings in the air holes. In order to propagate OAM modes stably, the PCFs should have low and flat dispersion (Xu et al. 2021), large effective mode area (Shen et al. 2020), small nonlinear coefficient (Liu and Zheng 2008), and large effective index difference between the circular scope and cladding (McMorran Benjamin et al. 2017). Recently, several types of optical fibers have been designed to transmit OAM modes. For example, Y. Yue et al. reported an annular PCF based on As_2S_3 with a large effective index difference of 3.35×10^{-2} (Yue et al. 2012a) and N. Ashok et al. described a PCF in which the dispersion in very mode was less than 300 ps/(nm·km) (Nandam 2018). X.G. Zhang et al. described a circular PCF in which the chromatic dispersion for OAM modes was within 39 ps/(nm·km) for a bandwidth of 750 nm (Wei Tian et al. 2016). F. Wang et al. proposed a PCF with mixed air holes to improve the air permeability for bigger effective index difference (Wang et al. 2016) and another PCF with a large effective mode area was also described (Bozinovic and Ramachandran 2011).

In the design of optical fibers, the properties can be improved by optimizing the various structural parameters. However, systematic and comprehensive studies of the influence of the structural parameters such as size on the characteristics of optical fibers performance have been rare. Moreover, there is little information on a simple and feasible optimization method for optical fibers pertaining to the propagation of OAM modes. At present, the common knowledge is that the relevant factors affecting transmission of OAM modes in PCFs include the effective refractive index, photon confinement ability, and light field distribution in the annular region (Brunet et al. 2014; Zhang et al. 2015; Brunet and Rusch 2016; Xu et al. 2011). In order to design optical fibers with better properties, it is necessary to have a simple and rational method to optimize parameters such as the thickness of the annular area. There are two ways to alter the thickness of the annular area. The first means is to change the distance between the first layer air hole and center air hole without adjusting the radius of the center air hole, and the second one is to change the radius of the central air hole without adjusting the position of the air hole. Herein, the effects of the effective index, effective index difference, dispersion, effective mode area, nonlinear coefficient, numerical aperture, mode purity, and walk-off length, and thickness of the annular area on the transmission of OAM modes in PCFs are investigated systematically. Our results reveal that the simple method and results have great value in the design and optimization of PCFs for transmission of OAM modes.

2 PCF design and numerical simulation method

To assess the effects of the thickness of the annular area on the fiber properties, a simple and common PCF structure is chosen as shown in Fig. 1. The background materials are silica (orange area) and the core is a big hole filled with air. The blue region composed of silica is

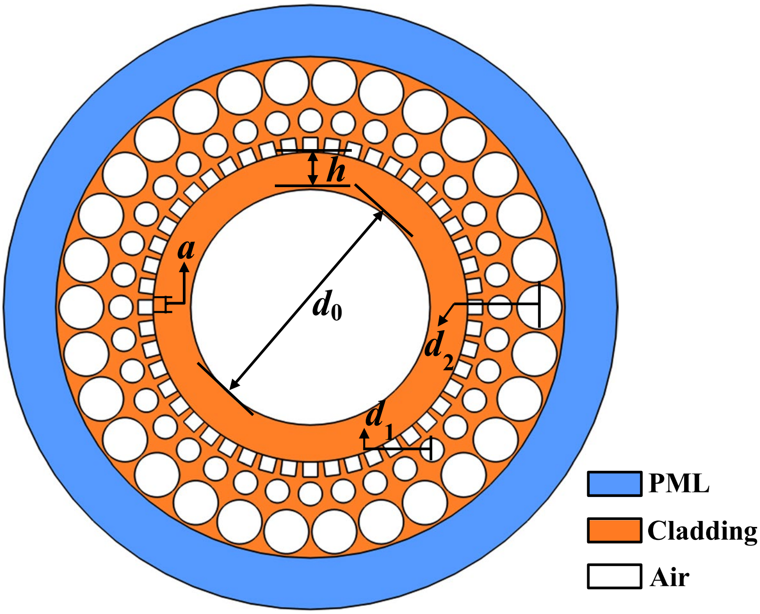

Fig. 1 Cross-section of the annular index profile structure in the photonic crystal fiber

the perfectly matched layer (PML) which limits the boundary conditions in the simulation. Two circular layers and one square layer of air holes are designed in the cladding of PCF. The reason why the difference in the diameters of the two layers of circular air holes is large is to reduce the confinement loss. The inner portion is a stratum of square air holes which not only increase air transmittance, but also concentrate the energy in the annular region. Therefore, the effective refractive index difference can give rise to stable transmission. In the structure, $d_1 = 0.8$ µm and $d_2 = 1.5$ µm are the diameters of the central and two kinds of circular air holes, respectively. The side length of the square air holes is $a = 1$ µm and h is the distance between the square and central air holes. It is noted that d_0 and h jointly determine the thickness of the annular area and propagation of OAM modes in the structure.

The refractive index of the background materials and PML depends on the Sellmeier equation (Liu 2015) as shown in Eq. (1):

$$n^2(\lambda) = 1 + \frac{A_1\lambda^2}{\lambda^2 - B_1} + \frac{A_2\lambda^2}{\lambda^2 - B_2} + \frac{A_3\lambda^2}{\lambda^2 - B_3} \tag{1}$$

where $A_1 = 0.6961663$, $A_2 = 0.4079426$, $A_3 = 0.897479$, $B_1 = 0.0684043$, $B_2 = 0.1162414$, and $B_3 = 9.896161$. The simulation is carried out using COMSOL to calculate the effective refractive index and other physical quantities and MATLAB is utilized for post-processing of some of the fiber characteristics.

3 Results and discussion

Two optimization methods are adopted to investigate the relationship between the thickness of the annular region and effective refractive index, effective index difference, effective mode area, nonlinear coefficient, effective index difference, and dispersion at a wavelength of 1.55 µm. The value of d_0 is fixed when h is changed and the distance between the square air hole to the center of the fiber is kept constant as d_0 is adjusted. Overall, the thickness of the annular area is varied between 2 and 2.5 µm.

3.1 Transmission modes

The OAM modes in optical fibers consist of the odd and even modes of the same order, meaning that OAM$\pm\pm l,m$ is composed of HEeven $l+1$ and HEodd $l+1$, or EHeven l-1 and EHodd l-1, where HE^{even} or EH^{even} is the even HE and EH modes and HE^{odd} or EH^{odd} is the odd mode of HE and EH modes, respectively. There is a $\pi/2$ phase difference between the odd and even modes and the number of OAM modes is determined by the following equations Kabir (2020):

$$\boldsymbol{OAM^{\pm}_{\pm l,m} = HE^{even}_{l+1,m} \pm iHE^{odd}_{l+1,m}} \quad \text{and} \quad \boldsymbol{OAM^{\mp}_{\pm l,m} = EH^{even}_{l-1,m} \pm iEH^{odd}_{l-1,m}} \tag{2}$$

where '$\pm$' in the upper right corner represents the right and left rotation directions of the circularly polarized OAM and 'l' is the topological charge of the OAM modes to indicate the order of OAMs in the fiber. Moreover, '$\pm$' before l is the direction of phase rotation and m, usually taken one, is the number of concentric circles about the intensity distribution of OAM modes in the radial direction. It can only be used as two information states because $OAM_{\pm 1,1}$ has the same circular polarization and rotation direction when $l=1$.

Theoretically the HE modes and EH modes can be linked to the OAM modes in the COMSOL simulation. $OAM_{1,\,m}$ has only two information bearing states and so it always has the same circular polarization and rotation directions (Zhu et al. 2017). Meanwhile, the higher-order OAM modes can produce four independent information bearing modes and they can polarize and rotate in the same or opposite direction (Alexeyev et al. 1998). The topological charge of the HE module can reach 8 and that of EH is up to 6 in this structure. Consequently, this fiber can transmit $6\times4+2=26$ OAM modes including OAM$\pm\pm$1,1{$HE_{2,1}$}, OAM$\pm\pm$2,1{$HE_{3,1}$,$EH_{1,1}$}, OAM$\pm\pm$3,1{$HE_{4,1}$,$EH_{2,1}$},

OAM$\pm\pm$4,1{$HE_{5,1}$,$EH_{3,1}$}, OAM$\pm\pm$5,1{$HE_{6,1}$,$EH_{4,1}$},OAM$\pm\pm$6,1{$HE_{7,1}$,$EH_{5,1}$},OAM$\pm\pm$7,1{$HE_{8,1}$,$EH_{6,1}$}. Among them, $HE_{3,1}$, $HE_{5,1}$, $HE_{8,1}$, $EH_{1,1}$, $EH_{3,1}$, $EH_{6,1}$ are selected for discussion.

Figure 2a to f show the field distributions in the z direction for a part of the modes at 1.55 µm. Because the EH modes are closer to the fiber core than HE modes, the OAM modes of the EH modes are more stable than those of HE under an external influence. Figure 2g to i indicate the phase distributions of the OAM modes which change π/2 azimuthally and therefore, these modes can be de-multiplexed with conjugating phase modes.

3.2 Effective refractive index

The effective index of the OAM modes determines the effective index difference and dispersion and the effective refractive index of the modes can be changed by adjusting the

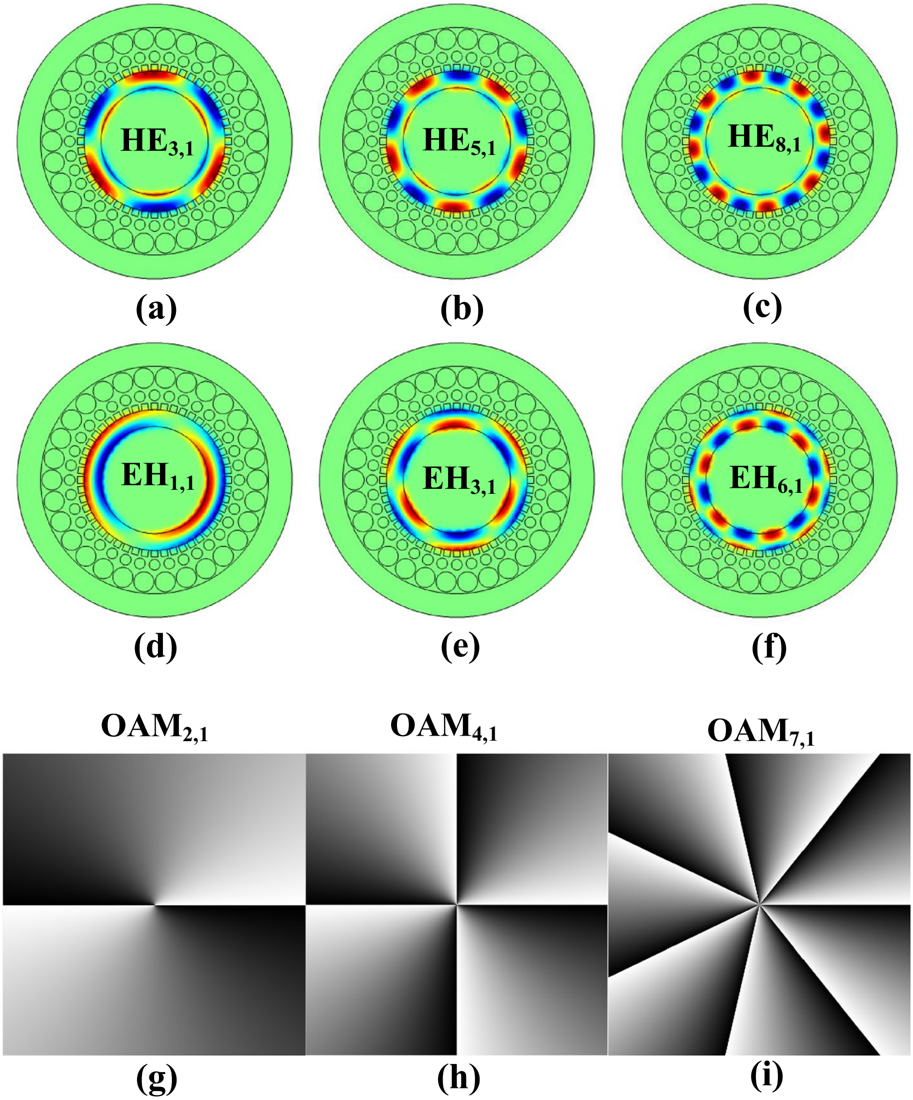

Fig. 2 **a**–**f** Optical field distributions of the partial HE and EH modes in the *z* direction at 1.55 μm; **g**–**i** Phase diagrams of the partially displayed OAM modes

thickness of the ring region. Figure 3a and b show the effects of the thickness of the annular region on the effective refractive index according to the two optimization methods described in this paper.

It has been shown that the higher the mode order, the lower is the effective refractive index (Liu et al. 2019; Zhang et al. 2016, 2017; Wang et al. 2020; Zhu et al. 2015). Therefore, only $HE_{3,1}$, $HE_{5,1}$, $HE_{8,1}$, $EH_{1,1}$, $EH_{3,1}$, and $EH_{6,1}$ are selected to discuss the mode functions. Figure 3 shows that the effective refractive index increases with increasing distance between the square and central air holes (h) but decreases with increasing radius of

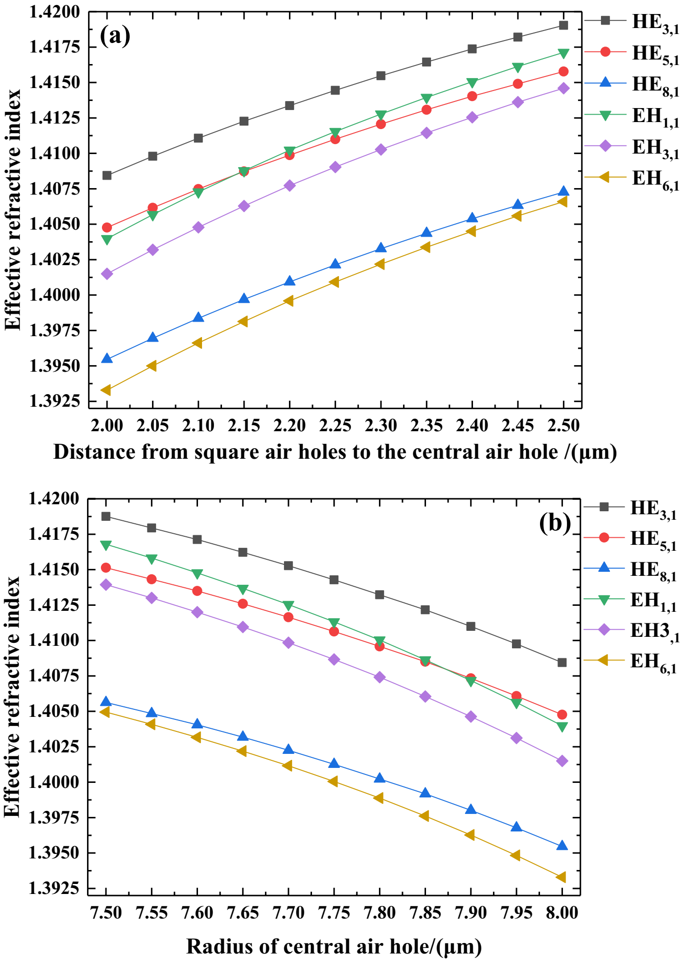

Fig. 3 **a** Effective refractive index obtained by changing the distance between the square and central air holes at 1.55 μm; **b** Effective refractive index obtained by changing the radius of the center air hole

the center air hole (d_0). The effective refractive index diminishes gradually. In addition, the trend shown in (a) is almost symmetrical with that in (b) because the variation range of the annular region thickness is consistent (2.0 μm to 2.5 μm) in the two optimization methods.

The effective index difference between the HE modes and EH modes should be greater than 1×10^{-4} (Bai et al. 2020) in order to transmit OAM modes stably in the optical fiber. An effective index difference of less than 1×10^{-4} may lead to crosstalk and coupling of different modes forming scalar LP modes (Wang et al. 2020). The relationship between the distance between the square air holes and central air hole (h), radius of the central air hole (d_0), and effective index difference in Fig. 4a and b indicates that the effective index difference is inversely proportional to h and directly proportional to d_0.

Similar to Fig. 2, the trend in Fig. 3a is almost symmetrical with that in (b). The effective index difference decreases with increasing annular area thickness and is eventually less than 1×10^{-4} so that it cannot be magnified without limit during optimization. Besides, to

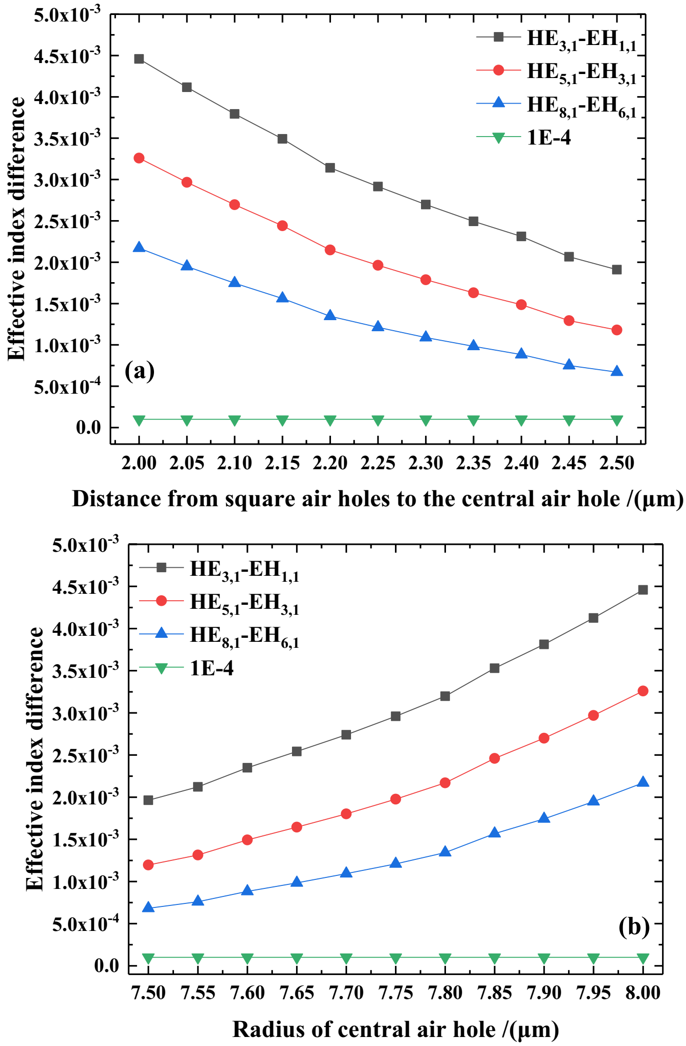

Fig. 4 **a** Effective index difference by changing the distance between the square air holes and central air hole at 1.55 μm. **b** Effective index difference by changing the radius of the central air hole

reduce crosstalk between different modes and ensure stable transmission of OAM modes, the radius of the central air hole can be increased appropriately to obtain a larger effective index difference.

3.3 Chromatic dispersion

Dispersion refers to the phenomenon of optical pulse broadening caused by different group velocities of different frequencies in the light source and it is divided into materials and waveguide dispersions (Huang et al. 2020). Because the effective index difference of the

OAM modes is greater than 1×10^{-4}, the dispersion is mainly composed of waveguide dispersion and determined by Eq. (3) (Ye et al. 2013):

$$D = -\frac{\lambda}{c}\frac{d^2Re\left(n_{eff}\right)}{d\lambda^2} \tag{3}$$

where $c=3\times10^8$ m/s is the speed of light, λ is the wavelength, and $Re(n_{\mathrm{eff}})$ is the real part of the effective refractive index. The dispersion curves in Fig. 5a and b describe the variations in the two cases when changing the thickness of the annular area at 1.55 µm.

Regardless of whether the distance between the square air holes and central air hole is increased or the radius of the central air hole is reduced, there is little difference between the HE modes. A part of light will return to the core for further transmission after entering the cladding through the interface between the core and cladding. Light

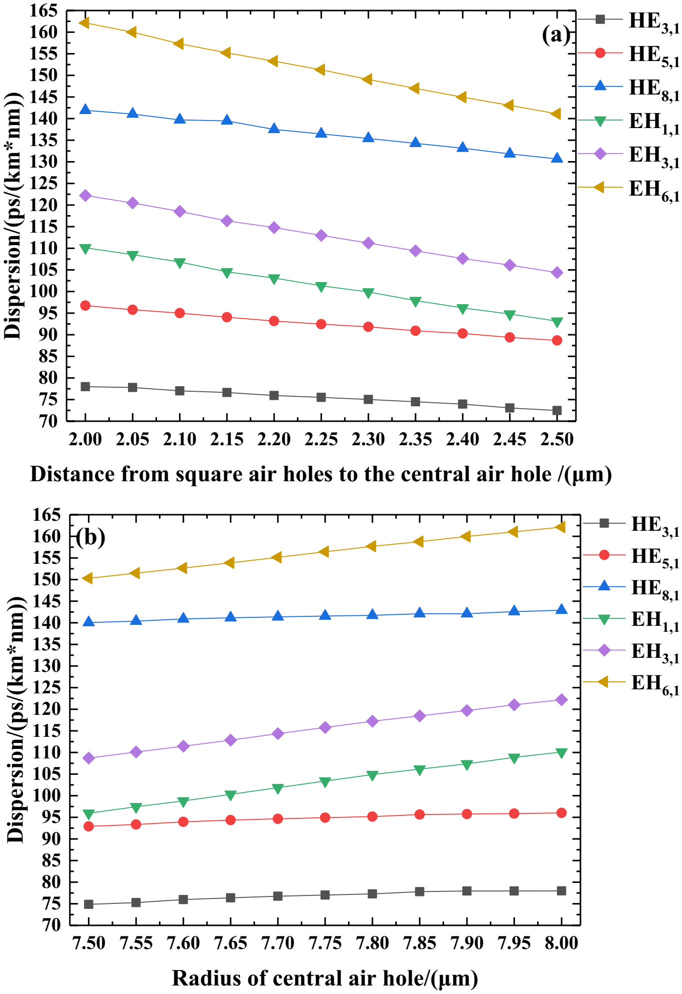

Fig. 5 **a** and **b** Variations of dispersion in the two ways by adjusting the thickness of the annular region

propagation in the cladding is faster than that in the core leading to pulse broadening and dispersion (Ademgil and Haxha 2008). Figure 5 shows that the two optimization methods have little effect on the dispersion of low-order EH modes, while the area of the annular region increased by reducing the radius of the central air hole is less than that increased by adding the distance between the square air hole and the central air hole, which can not reduce the dispersion of higher-order modes more. Consequently, it is more efficacious to increase the thickness of the annular area by increasing the distance between the square air holes and central air hole in order to debase dispersion.

3.4 Effective mode area and nonlinear coefficient

The area of the high refractive index ring region is called the effective mode area, which can be used to express the photon energy concentration in the optical fiber. The effective mode area which is inversely proportional to the photon energy concentration can be calculated by Eq. (4) (Kabir et al. 2020a):

$$A_{eff} = \frac{\left(\iint |E(x,y)|^2 dxdy\right)^2}{\iint |E(x,y)|^4 dxdy} \tag{4}$$

where $E(x,y)$ is the electric vector of the cross-section of the optical fiber in light propagation, which can be studied by COMSOL directly. Another important physical quantity inversely proportional to the effective mode area is the nonlinear coefficient which can be calculated by Eq. (5) (Bai et al. 2018):

$$\gamma = \frac{2\pi n_2}{\lambda A_{eff}} \tag{5}$$

where $n = 2.3 \times 10^{-20} \mathrm{m}^2 \cdot \mathrm{W}^{-1}$ is the nonlinear refractive index of silica, λ is the wavelength, and A_{eff} is the effective mode area. The nonlinear coefficient is a physical quantity that characterizes the influence of the nonlinear effects on the optical fiber. The nonlinear effects refer to those caused by nonlinear polarization of the medium under the action of strong light due to the small size of the optical fiber and mainly include stimulated absorption and refractive index disturbance. The smaller the nonlinear coefficient, the better is transmission of the OAM modes and therefore, the effective mode area should be as large as possible. Figure 6a–d show the effective mode areas and nonlinear coefficients for the two optimization ways.

The effective mode area is proportional to the thickness of the annular region. The reason why increasing thickness of the annular region can expand the area of the light guide in the fiber and the effective mode field area will enlarge accordingly is that the optical energy is mainly concentrated in the ring region, so that the nonlinear effects are depressed to transmit the OAM modes steadily. It is also better to increase the thickness of the annular region by enlarging h because a large core radius has stronger binding ability with photons consequently reducing the possibility of photons leaking into the cladding to exacerbate the nonlinear effects. Consequently, it is more advantageous to increase the distance between the square and central air holes when optimizing the fiber structure.

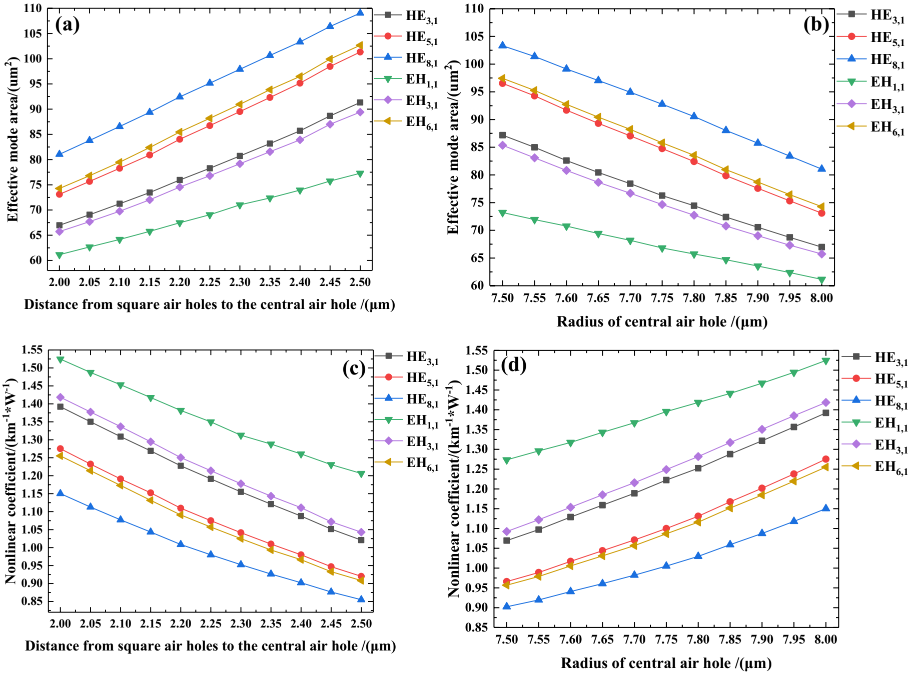

Fig. 6 **a–d** Effective mode areas and nonlinear coefficients for the two optimization ways

3.5 Numerical aperture (NA)

The numerical aperture (NA) describes the cone angle of light entering and leaving the fiber. NA is a dimensionless entity representing the ability of the optical fiber to receive and transmit light. It can be utilized to measure the total acceptance of optical power into the fiber and calculated by Eq. (6) (Kabir et al. 2020b):

$$NA = \left(1 + \frac{\pi A_{eff}}{\lambda^2}\right)^{\left(-\frac{1}{2}\right)} \tag{6}$$

where A_{eff} is the effective mode area and λ is the wavelength. NA is inversely proportional to the area of the effective mode field and directly proportional to the wavelength. Theoretically, it is better to have a larger numerical aperture. Figure 7a and b exhibit the relationship between the thickness of the annular region and NA for the two cases. The two ways to increase the thickness of the annular area will reduce NA, but it is better to change the radius of the central air hole. This is because for the same thickness, NA is relatively large and conducive to the optical power coming in and out of the fiber.

3.6 OAM purity

The OAM purity is an important parameter of the PCF in optical communication because only the modes with high purity can be transmitted stably in the fiber. In fact, the mode purity (η) is more important in large capacity transmission. The purity of the OAM modes

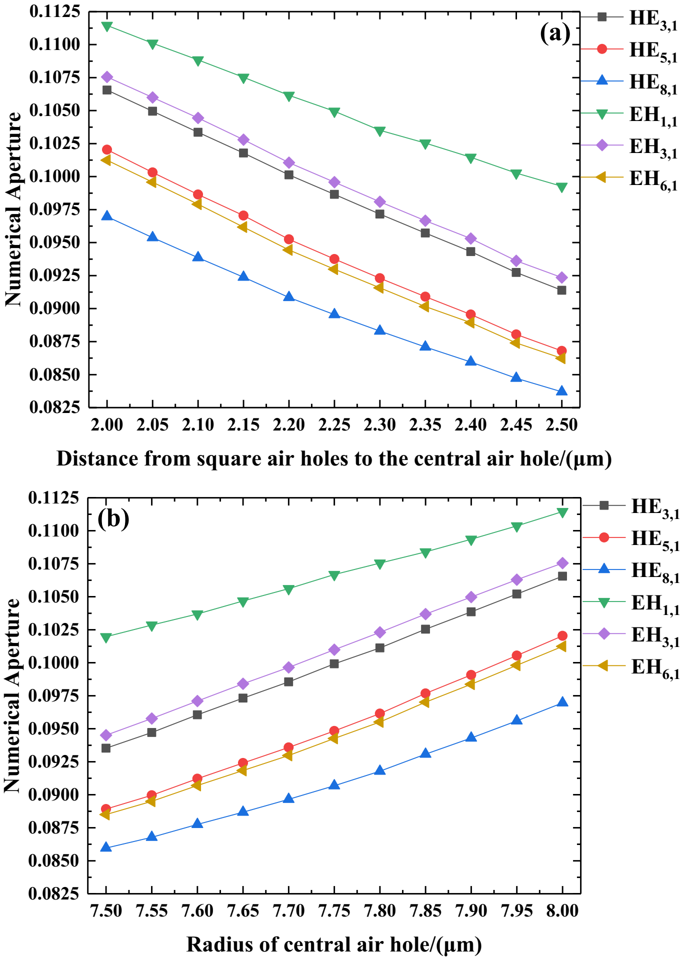

Fig. 7 **a** and **b** Relationship between the thickness of the annular region and NA for thein two cases

can be qualitatively evaluated using the light intensity overlap factor as shown in Eq. (7) (Fahad and Ahmed 2020):

$$\eta = \frac{I_r}{I_c} = \frac{\iint_{\text{ring}} \left|\overrightarrow{E}\right|^2 dxdy}{\iint_{\text{cross - section}} \left|\overrightarrow{E}\right|^2 dxdy} \tag{7}$$

where I_r and I_c are the light intensity of the ring area and entire fiber section, respectively, which can be computed by COMSOL. The purity of the OAM modes at 1.55 μm is presented in Fig. 8a and b for different ring area thicknesses for the two ways.

The higher the mode purity, the more stable is the transmission. By adjusting the thickness of the annular region, the mode purity increases. A higher mode purity can be obtained by changing the radius of the central air hole under the same conditions. The mode purity of the HE mode is more important than that of the EH mode because the

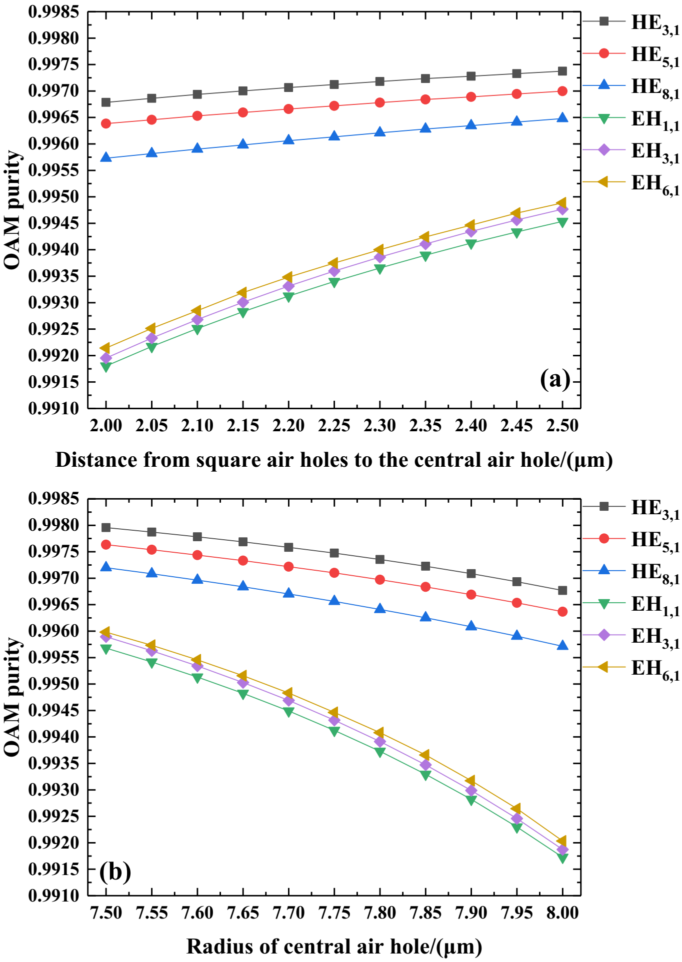

Fig. 8 **a** and **b** Purity of a part of the OAM modes

EH mode is closer to the core and the optical energy of the EH mode in the ring region is lower. Hence, the radius of the central air hole can be reduced to improve the mode purity when optimizing the structure.

3.7 Walk-off length

The different transmission velocities of the odd and even modes of the same order OAM mode in the fiber lead to walk-off effect. The length of walk-off determines the mode transmission distance in the optical fiber and is proportional to the transmission distance. When the faster mode and slower mode are separated by a certain distance due to the walk-off effect, the OAM modes cannot be synthesized normally. The walk-off length of 2π ($L_{2\pi}$) and walk-off length of 10 *ps* (L_{10ps}) can be used to analyze the walk-off effect. $L_{2\pi}$ is the propagation distance of two eigenmodes at an interval of 2π optical periods and L_{10ps} is the delay propagation distance of two eigenmodes separated by 10 ps. Equations (8) and (9) (Yue et al. 2012b) are used to calculate the two kinds of walk-off length at 1.55 μm:

$$L_{2\pi} = \frac{\lambda}{n_{eff}^{even} - n_{eff}^{odd}}(m) \tag{8}$$

$$L_{10ps} = \frac{c \times 10ps}{n_{eff}^{even} - n_{eff}^{odd}} = \frac{3 \times 10^{-3}}{n_{eff}^{even} - n_{eff}^{odd}}(m) \tag{9}$$

where λ is the wavelength, c is the speed of light and *neven eff* and *nodd eff* are the effective index differences of the even and odd modes, respectively. Figure 9a–d show the two kinds of walk-off lengths for different annular thickness. Although there is no obvious relationship between the thickness of the annular region and two types of walk-off lengths, adjusting the radius of the central air hole for the same thickness can obtain a larger walk-off length and transmission over a longer distance in the optical fiber.

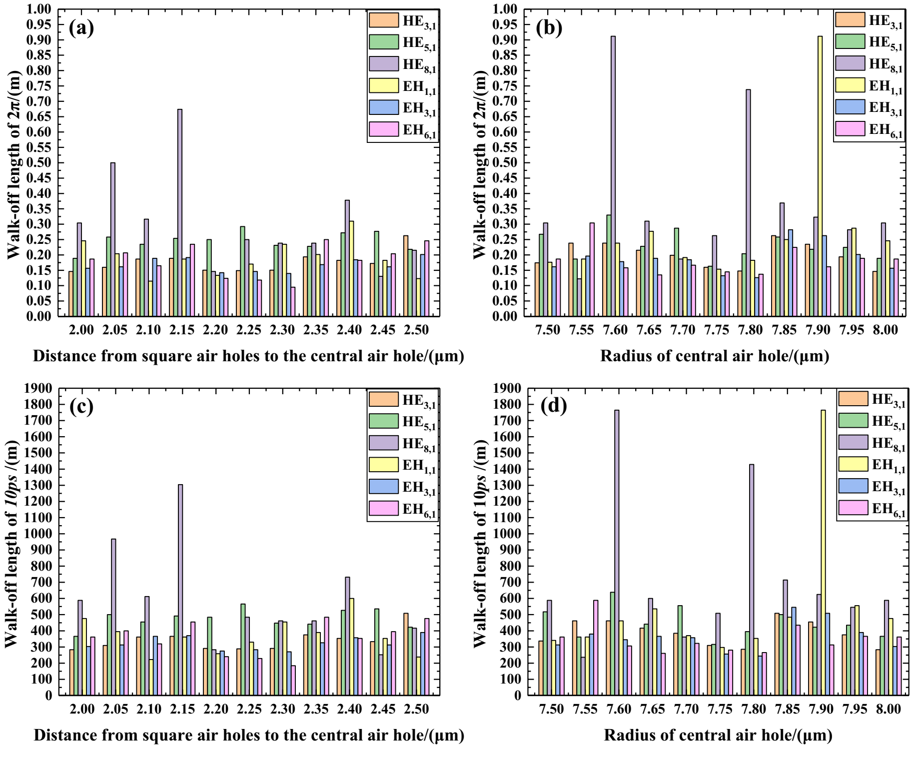

Fig. 9 **a**, **b** Walk-off length of 2π and **c**, **d** walk-off length of 10 *ps*

3.8 Confinement loss

The confinement loss which can not only determine the mode quality, but also affect the stable transmission of OAM modes is a significant parameter of the PCF. In addition, the lower the confinement loss is, the longer the stable transmission distance of OAM modes is. The confinement loss is determined by Eq. (10) (Hassan et al. 2020):

$$L = \frac{2\pi}{\lambda}\frac{20}{\ln(10)}10^6 Im\left(n_{eff}\right) \tag{10}$$

where λ is the wavelength and Im(neff) is the imaginary part of effective refractive index.

Figure 10 shows the effects of two different optimization methods on confinement loss. It is seen from Fig. 10 that there is no obvious relationship between the confinement loss and the thickness of the annular region. However, a lower confinement loss up to

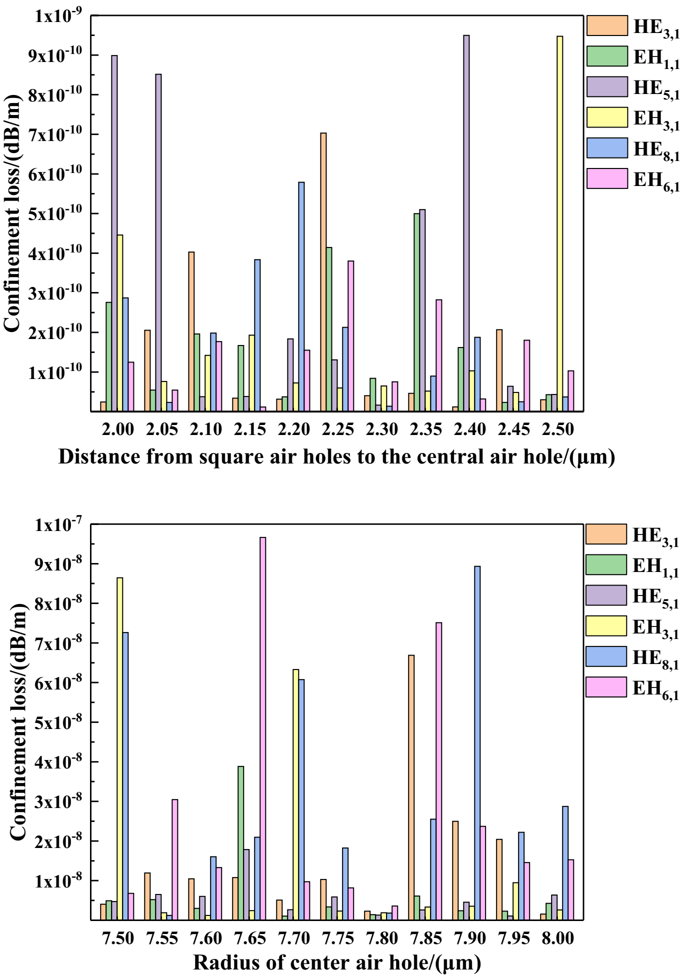

Fig. 10 **a**, **b** Confinement loss in two optimization methods

Table 1 The prime parameters of the PCF

Parameter	a	d_0	d_1	d_2	h
Numerical value	1 μm	7.5 μm	0.8 μm	1.5 μm	2.5 μm

10–9-10–11 dB/m can be obtained by increasing the distance between square air holes and the central air hole. Consequently, increasing this distance has advantage of reducing the confinement loss.

3.9 Final structure

In the previous content, through two optimization methods, the influences of the thickness of the annular region on effective refractive index, effective index difference, dispersion, effective mode area, nonlinear coefficient, NA, OAM purity, walk-off length and confinement loss are calculated, and some conclusions are obtained. In this section, the structure shown in Fig. 1 has been optimized, and we design the PCF with the best performance. The main parameters of the PCF are listed in Table 1.

The performances of the PCF with optimized structure are calculated at 1.55 μm by using COMSOL Multiphysics software and are listed in Table 2.

The simulation at 1.55um indicates that the effective refractive index difference of all OAM modes is greater than 1×10^{-4}, which ensures the stable transmission of OAM modes. The minimum dispersion and lowest nonlinear coefficient are only 61.87 ps/(km·nm) ($HE_{1,1}$) and 0.765 $km^{-1} \cdot W^{-1}$, respectively. In addition, the purity of all OAM modes is larger than 99.76% and the confinement loss is between 10^{-11} and 10^{-9} dB/m, thus the OAM modes will hardly leak into the cladding. Moreover, the maximum 10 ps walk-off length of the proposed PCF is 5803 ($HE_{6,1}$), which can be used for long-distance propagation.

4 Conclusion

By adjusting the thickness of the annular area, transmission of OAM modes in PCFs can be optimized to provide the theoretical foundation for the design of optical fibers. For the thickness range of the annular area between 2.0 and 2.5 μm, the radius of the central air hole or distance between the square air holes and central air hole can be varied from 2.0 to 2.5 μm and 8.0 to 7.5 μm, respectively. By means of simulation and comparative analysis, the effective index difference, dispersion, nonlinear coefficient, and NA are inversely proportional to the thickness of the annular area, but the effective mode area and OAM purity are directly proportional to the thickness of annular area. In particular, the distance between the square air holes and central air hole is the better parameter for optimization of the dispersion, effective mode area, and nonlinear coefficient, whereas the radius of the central air hole is more suitable for optimizing the NA, OAM purity and walk-off length. The method and results provide useful information to optimize optical fibers for transmission of OAM modes.

Table 2 Various properties of PCF at 1.55 μm

OAM modes	$HE_{1,1}$	$HE_{2,1}$	$HE_{3,1}$	$HE_{4,1}$	$HE_{5,1}$	$HE_{6,1}$	$HE_{7,1}$
Effective refractive index	1.42666	1.42613	1.42512	1.42356	1.42143	1.41871	1.41541
Dispersion/(ps/(km·nm))	61.87	64.9	70.19	77.93	88.29	101.42	117.48
Effective mode area/(μm^2)	90.481	101.99	110.38	115.49	118.61	120.6	121.93
Nonlinear coefficient/($km^{-1}\cdot W^{-1}$)	1.031	0.914	0.845	0.807	0.786	0.773	0.765
NA	0.092	0.086	0.083	0.081	0.08	0.079	0.079
OAM purity	0.9989	0.9987	0.9986	0.9985	0.9984	0.9983	0.9982
10 ps walk-off length(m)	875	905	1500	1367	1636	5803	2538
Confinement loss/(dB/m)	2.09×10^{-10}	1.54×10^{-11}	5.21×10^{-10}	1.82×10^{-11}	8.78×10^{-11}	3.14×10^{-10}	3.14×10^{-09}
OAM modes	$HE_{8,1}$	$EH_{1,1}$	$EH_{2,1}$	$EH_{3,1}$	$EH_{4,1}$	$EH_{5,1}$	$EH_{6,1}$
Effective refractive index	1.41151	1.42412	1.42286	1.42089	1.41829	1.41506	1.41123
Dispersion/(ps/(km·nm))	136.55	82.36	87.62	96.18	107.92	122.74	140.56
Effective mode area/(μm^2)	122.85	89.03	100.47	108.83	113.95	117.05	118.98
Nonlinear coefficient/($km^{-1}\cdot W^{-1}$)	0.759	1.047	0.928	0.857	0.818	0.797	0.784
NA	0.079	0.092	0.087	0.084	0.082	0.081	0.08
OAM purity	0.9981	0.9975	0.9976	0.9977	0.9977	0.9977	0.9976
10 ps walk-off length(m)	3492	961	939	1265	1158	1176	1979
Confinement loss/(dB/m)	1.09×10^{-11}	8.05×10^{-11}	5.19×10^{-10}	1.71×10^{-10}	2.47×10^{-10}	3.65×10^{-10}	1.84×10^{-10}

OAM modes	$OAM_{2,1}$	$OAM_{3,1}$	$OAM_{4,1}$	$OAM_{5,1}$	$OAM_{6,1}$	$OAM_{7,1}$
Effective index difference	9.99×10^{-04}	7.03×10^{-04}	5.37×10^{-04}	4.28×10^{-04}	3.47×10^{-04}	2.78×10^{-04}

Acknowledgements This work was jointly supported by Local Universities Reformation and Development Personnel Training Supporting Project from Central Authorities [140119001], City University of Hong Kong Strategic Research Grant (SRG) [Grant Numbers 7005105 and 7005265], and Scientific Research Fund of Sichuan Province Science and Technology Department [2020YJ0137].

Funding We declare that we have no financial and personal relationships with other people or organizations that can inappropriately influence our work, there is no professional or other personal interest of any nature or kind in any product, service and or company that could be construed as influencing the position presented in, or the review of, the manuscript entitled 'Optimization of photonic crystal fibers for transmission of orbital angular momentum modes'.

Declarations

Conflict of interest The authors declare no conflicts of interest.

References

Ademgil, H., Haxha, S.: Highly birefringent photonic crystal fibers with ultralow chromatic dispersion and low confinement losses [J]. J. Lightwave Technol. **26**(4), 441–448 (2008)

Alexeyev, A.N., Fadeyeva, T.A., Volyar, A.V., et al.: Optical vortices and the flow of their angular momentum in a multimode fiber. Semicond. Phys. **1**, 82–89 (1998)

Bai, X., Chen, H., Zhuang, Y., et al.: A new type Bragg fiber for supporting 50 orbital angular momentum modes [J]. Opt. – Int. J. Light Electron Opt. **219**, 165153 (2020)

Bai, X, Chen, et al.: Design of a circular photonic crystal fiber with square air-holes for orbital angular momentum modes transmission[J]. Optik: Zeitschrift fur Licht- und Elektronenoptik: = Journal for Light-and Electronoptic, 2018, 158:1266–1274

Bozinovic, N, Kristensen, P, Ramachandran, S.: Long-range fiber-transmission of photons with orbital angular momentum[C]. In: Lasers & Electro-optics. IEEE, (2011)

Brunet, C., Rusch, L.A.: Invited paper: optical fibers for the transmission of orbital angular momentum modes [J]. Opt. Fiber Technol. **31**, 172–177 (2016)

Brunet, C., Vaity, P., Messaddeq, Y., et al.: Design, fabrication and validation of an OAM fiber supporting 36 states[J]. Opt. Express **22**(21), 26117 (2014)

Fahad, A., Ahmed, K.: Novel design of dual guided photonic crystal fiber for large capacity transmission in high-speed optics communications with supporting good quality OAM and LP modes[J]. AEJ – Alex. Eng. J. **59**(6), 4889–4899 (2020)

Hassan, M.M., Kabir, M.A., Hossain, M.N., et al.: Numerical analysis of circular core shaped photonic crystal fiber for orbital angular momentum with efficient transmission[J]. Appl. Phys. B (2020). https://doi.org/10.1007/s00340-020-07497-2

Huang, W., et al.: A photonic crystal fiber for supporting 30 orbital angular momentum modes with low dispersion [J]. Optoelectron. Lett. **16**(1), 34–39 (2020)

Kabir, M.A., Ahmed, K., Hassan, M.M., Hossain, M.M., Paul, B.K.: Design a photonic crystal fiber of guiding terahertz orbital angular momentum beams in optical communication [J]. Opt. Commun. **475**, 126192 (2020)

Kabir, M.A., Hassan, M.M., Hossain, M.N., et al.: Design and performance evaluation of photonic crystal fibers of supporting orbital angular momentum states in optical transmission [J]. Opt. Commun. **467**, 125731 (2020a)

Kabir, M.A., Hassan, M.M., Ahmed, K., et al.: Novel spider web photonic crystal fiber for robust mode transmission applications with supporting orbital angular momentum transmission property[J]. Opt. Quant. Electron. (2020b). https://doi.org/10.1007/s11082-020-02447-w

Kibler, B., Lemière, A., Gomes, J.-T., Gaponov, D., Lavoute, L., Désévédavy, F., Smektala, F.: Octave-spanning coherent supercontinuum generation in a step-index tellurite fiber and towards few-cycle pulse compression at 2 [formula omitted][J]. Opt. Commun. **488**, 126853 (2021)

Liu, S., Zheng, H.: Measurement of nonlinear coefficient of optical fiber based on small chirped soliton transmission. Chin. Opt. Lett. **6**(07), 533–535 (2008)

Liu, C., Wang, F., Lv, J., Sun, T., Liu, Q., Mu, H., Chu, P.K.: Design and theoretical analysis of a photonic crystal fiber based on surface plasmon resonance sensing [J]. J. Nanophotonics **9**(1), 093050 (2015)

Liu, E., Tan, W., Yan, B., et al.: Robust transmission of orbital angular momentum mode based on a dual-cladding photonic quasi-crystal fiber [J]. J. Phys. D Appl. Phys. **52**(32), 325110 (2019)
Majumdar, A., Das, S., Gangopadhyay, S.: A simple method for prediction of effective core area and index of refraction of single-mode graded index fiber in the low V region[J]. J. Opt. Commun. (2014). https://doi.org/10.1515/joc-2014-0020
McMorran, B.J., Agrawal, A., Ercius, P.A., Grillo, V., Herzing, A.A., Harvey, T.R., Linck, M., Pierce, J.S.: Origins and demonstrations of electrons with orbital angular momentum. Philos. Trans. Ser. A Math. Phys. Eng. Sci. **375**(2087), 20150434 (2017)
Nandam, A., Shin, W.: Spiral photonic crystal fiber structure for supporting orbital angular momentum modes. Optik **169**, 361–367 (2018)
Ott, M.N., Proctor, M., Dodson, M., et al.: Optical fiber cable assembly characterization for the mercury laser altimeter[J]. Proc. SPIE – Int. Soc. Opt. Eng. **5104**, 96–106 (2003)
Ott M N, Larocca F, Thomes W J, et al.: Applications of optical fiber assemblies in harsh environments: The journey past, present, and future[C] In: Optical Engineering + Applications. (2008)
Rui-Chao L I, Zhang D.: The history, applications and future trends of fiber optical communication. Studies in Philosophy of Science and Technology, (2017)
Shen, X., Ding, J., Zhang, L., Wei, W.: A segmented heterostructure cladding fiber designed for extreme large mode area[J]. Optik **212**, 164708 (2020)
Tian, W., Zhang, H., Zhang, X., Xi, L., Zhang, W., Tang, X.: A circular photonic crystal fiber supporting 26 OAM modes[J]. Opt. Fiber Technol. **30**, 184–189 (2016)
Wang, W., Wang, N., Li, K., et al.: A novel dual guided modes regions photonic crystal fiber with low cross-talk supporting 56 OAM modes and 4 LP modes [J]. Opt. Fiber Technol. **57**, 102213 (2020)
Wang, W., Sun, C., Wang, N., et al.: A design of nested photonic crystal fiber with low nonlinear and flat dispersion supporting 30+50 OAM modes [J]. Opt. Commun. **471**, 125823 (2020)
Wang, F et al.: A new design of a circular photonic crystal fiber supporting 34 OAM modes[C]. In: Australian Conference on Optical Fibre Technology. (2016)
Xu, H., Wu, J., Xu, K., et al.: Ultra-flattened chromatic dispersion control for circular photonic crystal fibers[J]. J. Opt. **13**(5), 055405 (2011)
Xu, H., Kong, Q., Zhou, C.: Crossings in photonic crystal fiber with hybrid core and design of broadband dispersion compensating photonic crystal fiber[J]. Opt. Fiber Technol. **63**, 102485 (2021)
Ye, C., et al.: Highly birefringent photonic crystal fibers with flattened dispersion and low confinement loss [J]. Optoelectron. Lett. **9**, 45–48 (2013)
Yue, Y., et al.: Octave-spanning super continuum generation of vortices in a As2S3 ring photonic crystal fiber. Opt. Lett. **37**(11), 1889–1891 (2012a)
Yue Y, Yan Y, Ahmed N, et al.: Mode and propagation effects of optical orbital angular momentum (OAM) Modes in a Ring Fiber [J]. (2012b)
Zhang, Z., Gan, J., Heng, X., et al.: Optical fiber design with orbital angular momentum light purity higher than 99.9%. Opt. Express **23**(23), 29331 (2015)
Zhang, H., Zhang, X., Li, H., et al.: A design strategy of the circular photonic crystal fiber supporting good quality orbital angular momentum mode transmission [J]. Opt. Commun. **397**, 59–66 (2017)
Zhang X, Hu Z, Wei T.: A circular photonic crystal fiber supporting OAM mode transmission[C]. In: 2016 15th International Conference on Optical Communications and Networks (ICOCN). IEEE, (2016)
Zhu, M., Zhang, W., Xi, L., et al.: A new designed dual-guided ring-core fiber for OAM mode transmission [J]. Opt. Fiber Technol. **25**, 58–63 (2015)
Zhu, F., Huang, S., Shao, W., et al.: Free-space optical communication link using perfect vortex beams carrying orbital angular momentum (OAM)[J]. Opt. Commun. **396**, 50–57 (2017)